Impaired vitreous composition and retinal pigment epithelium function in the FoxG1::LRP2 myopic mice

Olivier Cases[a,b,c+], Antoine Obry[d,e+], Sirine Ben-Yacoub[a,b,c], Sébastien Augustin[a,b,c], Antoine Joseph[a,b,c], Géraldine Toutirais[f], Manuel Simonutti[a,b,c], Annabel Christ[g], Pascal Cosette[d] and Renata Kozyraki[a,b,c*]

Affiliations

[a] INSERM, U968, Paris, F-75012, France;

[b] UPMC Univ Paris 06, UMR_S968, Institut de la Vision, Paris, F-75012, France;

[c] CNRS, UMR_7210, Paris, F-75012, France;

[d] CNRS, UMR_6270, PISSARO Proteomics Platform, Institute for Research and Innovation in Biomedicine, Rouen University, Mont Saint Aignan F-76821, France;

[e] INSERM, U905, PISSARO Proteomics Platform, Institute for Research and Innovation in Biomedicine, Rouen University Hospital, Rouen F-76000, France;

[f] Plateforme de microscopie électronique, IBPS, UPMC Univ Paris 06, F-75005, France;

[g] Max-Delbrück-Center for Molecular Medicine, Berlin, D-13125, Germany.

Corresponding author: Renata Kozyraki; renata.kozyraki@inserm.fr

Authorship note: O. Cases and A. Obry contributed equally to the work

Abstract

High myopia (HM) is one of the main causes of visual impairment and blindness all over the world and an unsolved medical problem. Persons with HM are predisposed to other eye pathologies such as retinal detachment, myopic retinopathy or glaucomatous optic neuropathy, complications that may at least partly result from the extensive liquefaction of the myopic vitreous gel. To identify the involvement of the liquid vitreous in the pathogenesis of HM we here analyzed the vitreous of the recently described highly myopic *low density lipoprotein receptor-related protein 2* (*Lrp2)*-deficient eyes. Whereas the gel-like fraction was not apparently modified, the volume of the liquid vitreous fraction (LVF) was much higher in the myopic eyes. Biochemical and proteome analysis of the LVF revealed several modifications including a marked decrease of potassium, sodium and chloride, of proteins involved in ocular tissue homeostasis and repair as well as of ADP-ribosylation factor 4 (ARF4), a protein possibly involved in LRP2 trafficking. A small number of proteins, mainly comprising known LRP2 ligands or proteins of the inflammatory response, was over expressed in the mutants. Moreover the morphology of the LRP2-deficient retinal pigment epithelium (RPE) cells was affected and the expression of ARF4 as well as of proteins involved in degradative endocytosis was strongly reduced. Our results support the idea that impairment of the RPE structure and most likely endocytic function may contribute to the vitreal modifications and pathogenesis of HM.

Keywords: High myopia; Endocytosis; Vitreous; low density lipoprotein receptor-related protein 2.

1. Introduction

The human *LRP2* gene (2q23.3-3.1) encodes the multiligand endocytic receptor LRP2/Megalin, essential for the renal reabsorption of plasma proteins and the homeostasis of various vitamins and nutrients. Mutations in *LRP2* have been associated with the Donnai-Barrow syndrome, a rare genetic syndrome characterized by facial, skeletal and auditory findings, high myopia (axially elongated eyes) and low-molecular weight proteinuria [1,2]. Mutations in *LRP2* and high myopia were also described in patients with the Stickler syndrome suggesting that *LRP2* might directly be associated with the highly myopic phenotype. We indeed recently reported that *Foxg1-Cre* mediated ablation of the *Lrp2* gene in the ocular tissues resulted in excessively long eyes essentially due to increased vitreous chamber depth [3]. We moreover showed that the mutant eyes displayed several features of myopic retinopathy including chorioretinal atrophy, loss of retinal photoreceptors and posterior staphyloma as well as a decrease in retinal ganglion cell axons and progressive optic nerve atrophy, known causes of visual deterioration and blindness [3–6]. These data indicate that LRP2 expressed in the ocular tissues, mainly the retinal pigment (RPE) and ciliary body (CE) epithelia is necessary for normal eye growth and vision but do not identify the underlying mechanism.

A potential regulator of eye growth is the vitreous humor, the colorless, highly aqueous gel-like matrix that fills the posterior segment of the eye [7]. In addition to the structural components collagen and hyaluronic acid, the vitreous contains various low molecular weight solutes such as ions, glucose, lactate or proteins. Soluble vitreous proteins may be essential for local nutrient supply and coordination of the eye growth and modifications in their concentration may reflect or anticipate ocular states of health and disease [7,8].

Vitreous liquefaction, i.e. progressive increase in liquid vitreous occurring simultaneously with a decrease in gel volume, begins at the age of four years and is associated with normal vitreous ageing [7,9]. In highly myopic eyes vitreous liquefaction occurs earlier, it is more extensive and has been associated with the progression of myopia-associated pathologies including nuclear cataract, glaucoma and rhegmatogenous retinal detachment [4,5,10–14]. A fundamental alteration of the myopic vitreous biochemistry was proposed more than 50 years ago [15] and liquid vitreous modifications were identified in experimentally induced myopia in the chick [16,17]. However the electrolytic balance, soluble protein content and the pathogenic potential of the liquid vitreous in congenital HM are still unknown. Furthermore the origin of the liquid vitreous remains unclear although disruption of the blood-ocular barriers and the ensuing leakage of serum components were proposed to contribute to vitreous liquefaction in both myopic patients and animal models [18–20].

To answer these questions and gain some insight into the pathogenesis of the disease and its complications we here analyzed the liquid vitreous chamber content of the highly myopic *Lrp2*-deficient eyes, examined the morphology and endocytic function of the outer blood-retinal barrier forming RPE cells and identified ARF4 as a novel factor potentially involved in LRP2-mediated endocytosis.

2. Materials and Methods

2.1.Ethics statement

Animal procedures were conducted in strict compliance with approved institutional protocols (INSERM and comité d'éthique en experimentation animale Charles Darwin N°5, permit number 01519.01) and in accordance with the provisions for animal care and use described in the European Communities council directive of 22 September 2010 (2010/63/EU). Deep anesthesia for terminal procedures (perfusion) was provided with a ketamine/xylazine cocktail (80mg/10mg/kg).

2.2. Animals

Foxg1.Cre (129.Cg-*Foxg1*$^{tm1(cre)Skm}$/J) mice were purchased from the Jackson Laboratory (Bar Harbor, Maine). *Lrp2*$^{Lox/Lox}$ mice have been described elsewhere [3]. The average optical parameters of the *Lrp2*$^{FoxG1.cre\text{-}KO}$ at three-months were measured by In vivo Magnetic Resonance Imaging and were as previously described [3] (control mice: axial length = 3.50 mm; Equatorial diameter = 3.15 mm; Vitreous chamber depth = 1.00 mm; ***Lrp2***$^{\boldsymbol{FoxG1.cre\text{-}KO}}$: axial length = 5.00 mm; Equatorial diameter = 4.00 mm; Vitreous chamber depth = 2.50 mm).

2.3. Liquid vitreous humor collection

Three-month-old mice were euthanized by CO_2 inhalation followed by decapitation. Eyes were weighed, oriented posterior-side up in a Petri dish. Optic nerve was sliced to allow collection of the liquid vitreous. Using a micromanipulator (UltraMicroPump UMP3, World Precision Instrument, Sarasota, FL), a glass pipette with a tip broken to 4µm diameter was introduced into the posterior chamber through the head of the optic nerve of the eye *in situ*. The pipette was attached to a micro syringe pump controller (SYS-Micro4, World Precision Instrument, Sarasota, FL) permitting 5 millisecond pulses of suction to the back of the pipette. Vitreous humor of the posterior chamber was withdrawn. In general, 2.5 µl of clear vitreous

humor could be retrieved from each eye in control conditions. In mutant conditions up to 20 µl could be retrieved from one eye. Concerning the biochemical analysis, normal or mutant liquid humors were pooled to obtain a necessary 100 µl volume.

2.4.Vitreous gel collection

Three-month-old mice were euthanized by CO_2 inhalation followed by decapitation. Eyes were weighed. The scleral tissue posterior to the limbus was grasped and a microsurgical blade was used to make an incision in the cornea from limbus to limbus. The lens and the vitreous were eviscerated using a fine needle holder and the vitreous was carefully dissected and analyzed.

2.5. In vivo injection of tracers

Two-month-old mice (n = 3 for each genotype) were used to retro-orbital-injections with fluorochrome labeled-albumin (100µg/ml albumin from bovine serum diluted in PBS, Alexa Fluor® 488 conjugate, Thermofisher, USA) or –transferrin (50µg/ml transferring from human serum, Alexa Fluor® 488 conjugate, Thermofisher). Fifteen minutes after injection, contra-lateral eye was removed and frozen in isopentane. Serial frozen sections were directly processed for confocal microscopy.

2.6. Immunohistochemistry - Immunofluorescence

Adults (n = 5 for each genotype) were anesthetized and perfused transcardially with 4% PFA in 0.12 M phosphate buffer, pH 7.4. After perfusion, eyes were removed from the skull and postfixed overnight in fresh fixative. Serial frozen sections were processed for immunocytochemistry using sheep anti-Lrp2 (1/2000) and mouse anti-alpha smooth muscle actin (1/250; ab7817, Abcam), anti-occludin (1/100; OC-3F10, ThermoFisher). Alexa 488- or 594-conjugated antibodies (1:200, Invitrogen) were used for secondary detection. Nuclear

staining was achieved in Hoechst 33342. Fluorescent images were obtained using an Olympus confocal microscope (FV-1200-IX83).

2.7. Protein analysis

2.7.1. Samples

Vitreous samples were stored at −80°C until analyzed. Protein concentration of these samples was determined using the Bradford method. Twenty-five µg of samples were loaded in Laemmli buffer on 7% polyacrylamide gels and allowed for a short period of migration (1 h). After Coomassie staining, the protein band was excised and the proteins within the bands were reduced in 5mM dithiothreitol and cysteins were irreversibly alkylated in 25 mM iodoacetamide. After washing steps with water, gel bands were submitted to protein digestion (trypsin from Promega, 0.5 µg per band). Several steps of peptide extraction were then performed in H_20/CH_3CN solutions (1:1) acidified with TFA (1%) and the peptide fractions were combined and evaporated.

2.7.2. Liquid nanochromatography and mass spectrometry

For each sample, peptides were dissolved in 0.1% formic acid in water. All experiments were carried out with a linear quadrupole ion trap-Orbitrap mass spectrometer (LTQ Orbitrap Elite, Thermo Scientific) equipped with a nano-ESI source and coupled to a nanoliquid chromatrography (Easy-nLC II, Thermo Scientific). The sample was loaded onto an enrichment column (Cap Trap C_8, 0.5 x 2 mm, Michrom Bioresources) and the separation was performed by using a reversed phase column (C_{18}, L153, ID 5µm, 100 Å pore size, Nikkyo Technos, Japan). The gradient (mobile phase A: H_2O/0.1% FA; mobile phase B: CH_3CN/0.1% FA) was delivered at a flow rate of 300 nl/min for 120 min. Tryptic peptides were eluted from the reverse-phase column into the mass spectrometer, using a linear gradient from 2% to 45% of B. The capillary voltage was set at 1.5 kV and

the source temperature at 200 °C. The mass spectrometer was operated in the data-dependent mode. Survey full scan mass spectra (from m/z 300 to 2000) were acquired in the Orbitrap with a resolution of 30,000. The mass spectrometer selected the 20 most intense ions for fragmentation.

2.7.3. Protein identification

Raw data files were processed using Proteome Discoverer 1.4 software (Thermo Scientific). Peak lists were searched using the MASCOT search engine (version 2.2, Matrix Science) against the SwissProt database (Sprot 55.6.fasta) with taxonomy *Mus Musculus* (15746 sequences). Database searches were performed with the following parameters: trypsin specificity, 1 missed cleavage site allowed; variable modifications: carbamidomethylation of cystein, and oxidation of methionine. The parent ion and daughter ion tolerances were 10 ppm and 0.5 Da, respectively. The results were filtered by applying the identity threshold score of 20. The false positive rates (FDR) were obtained using a reverse database search approach ranged from 1.65 to 2.18 %. Within Proteome Discoverer, a further filtering step was applied: only peptides associated to "high confidence" (HC) were kept and at least two HC peptides were needed for protein identification.

2.7.4. Relative quantification by Progenesis LC-MS

Raw data were imported in Progenesis LC-MS software (v4.0.4441.29989). One sample was set as a reference, and the retention times of all other samples within the experiment were aligned. After alignment, data were normalized. Normalization results in a unique factor for each sample that corrects all peptides abundances in the sample. Statistical analysis was performed using normalized abundances for one-way analysis of variance (ANOVA) calculations. Features presenting p-value <0.05 and q-value <0.05 were

selected. MS/MS spectra from selected peptides were exported from the Progenesis LC-MS software as a mgf file and used for peptide identification. Search parameters were identical to those described above when using Proteome Discoverer. Conflicting features were discarded for quantification. The total cumulative abundance of the protein was calculated by summing the abundances of all peptides.

2.7.5. SDS-PAGE and Western blot analysis

Three-month-old mice (n = 5 for each genotype) were used. Retinal, RPE and vitreous lysates were prepared as previously described [3]. SDS-PAGE and immunoblotting were performed as previously described [3]. Briefly 15 μg of vitreous gel, retina or RPE were separated in 4-12% SDS-PAGE gels (Invitrogen) and transferred to nitrocellulose membranes. After blocking the membranes were incubated with the following primary antibodies: mouse anti-EAA1 (1/250; 610457, BD-transduction lab) and anti-collagen II (1/250; M2193, Santa Cruz), and rabbit anti-alpha smooth muscle actin (1/100; ab5694, Abcam), anti-fibrillin (1/500; sc-20084, Santa Cruz), anti-phospho Erk1-2 (Thr202-204; 1/1,000; 4376, Cell Signaling technology), anti-Erk1-2 (1/1,000; 4695, Cell Signaling technology), anti-LIMP2 (1/100; PA5-20540, ThermoFisher), anti-rab11 (1/200; sc-9020, Santa Cruz) and anti-ZO-1 (1/250; sc-10804, Santa Cruz), and goat anti-collagen alpha 1 (1/250; sc-8784, Santa Cruz) anti-fibronectin (1/250; sc-6952, Santa Cruz). Mouse anti-GAPDH (1/500; SC-166545, Santa Cruz) was used as an internal control. Immunoblots were washed in TBS–0.02% Tween 20 (TBST), incubated for 1 h with the appropriate horseradish peroxidase-coupled IgG (diluted 1:5000), washed in TBS–0.02% Tween 20, revealed using Super Signal (Pierce, Rockford, IL), and exposed to Hyperfilm ECL (Amersham Biosciences). Silver staining using the Biorad Silver Stain Plus kit was performed according to the manufacturer's instructions.

2.7.6. Immunoprecipitation

Normal RPE cell lysates (n = 3) were applied on Sepharose A or Sepharose G (GE Healthcare) beads coupled with anti-Lrp2 or anti-Arf4 antibodies. Immunoprecipitation was performed using standard procedures. Control immunoprecipitation was performed with sheep or mouse pre-immune serum. All precipitated proteins were analyzed by reducing SDS–PAGE and were detected by autoradiography using ECL reagents as described by the manufacturer (GE Healthcare).

2.8.Transmission Electron Microscopy

Three-month-old (n = 3 for each genotype) mice were anesthetized and perfused transcardially with 2% paraformaldehyde 2.5%glutaraldehyde in 0.1M PBS (pH 7.4). Retinas were sliced in 200-µm-thick sections, postfixed 2 h in 1% osmium tetroxide, dehydrated in alcohol, cleared in acetone, and embedded in Epon. For light microscopy, transverse serial sections (1 µm) were cut, heat dried, and stained with toluidine blue. Ultrathin sections were cut and stained with lead citrate and examined with a Philips (Aachen, Germany) CM100 electron microscope. For each genotype, three different animals were analyzed.

2.9. Blood sample collection

After an overnight fast, mice were shortly anesthetized with isoflurane (Forene^{r}, Abbot, France) and blood was collected at 9 a.m. by retro-orbital puncture. For biochemical analysis 300 µl of blood was collected into a heparinized tube.

2.10. Biochemical analyses

About 12 biochemical parameters were measured, including electrolytes and ions (sodium, potassium, chloride, calcium, iron) and other metabolites (creatinine, total protein, albumin, transferrin) in the blood as well as the liquid vitreous fraction. These parameters were

determined using an Olympus AU 400 analyzer (Beckman Coulter, Inc, Brea CA, USA) with kits and controls supplied by Olympus or other suppliers. The number of control and mutant eyes analyzed were 30 and 6 respectively. For all the samples three independent analyses were performed.

2.11. Data analyses and statistics

Data are expressed as the means ± s.e.m. Differences between the experimental groups were evaluated using ANOVA followed, when significant ($P < 0.05$), by the Tukey-Kramer test. When only two groups were compared, Mann-Whitney or Student's *t* test was used as appropriate. The statistical analyses were performed using Graph Prism Software and Sigmaplot.

3. Results

3.1. The electrolytic composition of the liquid vitreous fraction is modified in the $Lrp2^{FoxG1.cre\text{-}KO}$ mutants.

The excessive axial elongation of the *Lrp2*-deficient eyes is essentially due to the increased depth of the vitreous chamber [3], a feature of high myopia [5,21]. We previously showed that the major modifications of the vitreous chamber depth (VCD) occurred during the first three months of life (P90) and that at this age the mutant VCD was already 2.5-fold longer than the control one [3]. As a consequence, the mean mass of the *Lrp2*-deficient eye differed greatly from those displayed by control eyes at P90 (*Lrp2*-deficient: m = 42.15 $\pm$ 2.3 mg, n = 24; control: m = 24.15 $\pm$ 0.81, n = 28; p-value = 1.849 10^{-35}< 0.001). We therefore isolated the vitreous chamber content of P90 control and *Lrp2*-deficient eyes, as described in the material section and [22]. A gel-like and a clear with no visible blood or pigment, acellular LVF were obtained from both the control and *Lrp2*-deficient eyes. In control mice the vitreous chamber was essentially filled by a gel-like material attached to the lens; it also contained low amounts of a liquid vitreous. The mean mass of the retro-lental gel-like fraction or the lens of the *Lrp2*-deficient eye did not differ from those displayed by control eyes (*Lrp2*-deficient: lens, m = 6.02 $\pm$ 0.09 mg and vitreous gel, m = 9 $\pm$ 0.11 mg, n = 24; control: lens, m = 6.07 $\pm$ 0.8 mg and vitreous gel, m = 9.01 $\pm$ 0.12 mg, n = 28; lens, p-value = 0.289, vitreous gel, p-value = 0.992). Moreover, the biochemical composition of the gel was globally preserved as suggested by the normal expression of the main vitreous components collagen, fibrillin and fibronectin (Fig. 1A, B).

Remarkably, the volume of the mutant LVF was at least 8-fold higher at P90 (*Lrp2*-deficient: V = 18.5 $\pm$ 0.91 µl; control: V = 2.07 $\pm$ 0.15 µl; p-value = 3.48 10^{-54}<0.001). LVF was analyzed as in the schematic experimental work-flow described in Fig 1C. We first characterized the concentration of several soluble constituents including sodium, potassium, chloride, lactate, glucose as well as the total iron content (Table 1) and compared them to their respective serum levels. As expected the concentration of the circulating electrolytes was similar in control and mutant mice (Table 1) and the values were in accordance with previously published results [23]. The concentration of the same electrolytes in the LVF was different from that of serum: the sodium, potassium, chloride, lactate and glucose content was higher in both the control and mutant LVF, the calcium and phosphorus content was lower in both genotypes (Table 1). Comparative analysis of the control and mutant LVF showed however that whereas the levels of lactate and glucose were not modified, the potassium level was two-fold decreased in the mutants. A slight decrease was also observed in the sodium and chloride content of the mutant LVF. On the contrary, the calcium and phosphorus levels were at least two-fold increased in the mutant LVF. Of note the total iron content was dramatically increased in the mutant LVF and its total antioxidant capacity (i.e. protein thiols, vitamins A, E) [24,25] was decreased (Table 1). Finally, the osmolality of the mutant LVF was lower than that of the controls (307.8 mOsm/L versus 346.1 mOsm/L) and the total protein concentration of the control and mutant LVF was of 0.3 g/L and 0.9 g/L respectively (Table 1).

3.2. The proteome of the liquid vitreous fraction is modified in the Lrp2$^{FoxG1.cre\text{-}KO}$ mutants.

3.2.1. Mass spectrometry overwiew.

To investigate the proteome of the control and mutant LVF we used label-free liquid nano chromatography-mass spectrometry analysis. Three samples of each condition (normal sample corresponding to the pool of 10 LVFs and individual mutant sample) were analyzed independently by nanoLC-MSMS (biological replicates). Each sample was analyzed in duplicate only for evaluation of analytical robustness (technical replicates).

In order to evaluate the reproducibility of the experiments, different linear regressions were performed by plotting the logarithm of the number of peptide spectrum matches (PSMs) for different samples of the same group (Ci vs Cj for controls) and for samples from different groups (Mi vs Ci for mutant vs control) (Figure 2A-B). The regression coefficient measured to evaluate the robustness of the technical scenario between biological replicates was found around 0.970. Besides, the regression coefficient is highly lower when comparing samples from the 2 groups, already arguing for the different LVF protein content.

Using the so-called spectral counting semi-quantitative approach with highly stringent criteria (at least two unique matched peptides for each protein and an adjusted p-value < 0.05) nano-LC-ESI-MS/MS experiments identified 679 proteins in the control LVF and 366 in the mutant LVF including 312 proteins that were common in the two groups (Figure 2C, TableS1 for all peptide sequences, Table S2 for all protein identifications, Table S3 for all proteins found in normal LVF and Table S4 for all proteins found in mutant LVF). More than 80% of the proteins identified in the control LVF were previously reported in proteome studies of human and mouse vitreous [26–31], validating our approach. Of the 679 proteins identified by mass spectrometry in controls, the majority concerned house-keeping metabolic pathways such as glycolysis or gluconeogenesis, but also more specific ones such as phagosome maturation. Interestingly, proteins involved in vision and recently inventoried in proteomic studies of the vitreous were also identified, including opticin, cystatin C, retinol-binding protein, protein dickkopf homolg 3 or S-arrestin [29].

When discarding proteins common to control and mutants samples, it resulted that 367 proteins appeared unique to the control LVF. Among the latter, proteins involved in ubiquitination process and phagosome maturation were the more represented pathways. In addition, numerous components directly or indirectly involved in the cytoskeleton dynamics (actin, septins, coronins …) were specifically observed in control LVF. Interestingly, all the 8 components of the T-complex, a multimeric chaperonin dedicated to ATP-dependent protein folding and in particular to folding of cytoskeleton proteins (including actin and tubulin)[32] were also present in this list.

3.2.2. Differential Expression

Nowadays, MS1-based measurements are considered more accurate than spectral counting in terms of sensitivity and also dynamic range. Accordingly, protein abundance in the LVF of control and mutant samples was compared using a 2–way ANOVA from the MS1-based measurement. This resulted in 387 proteins displaying decreased abundance and in 74 proteins displaying increased abundance when mutant samples were compared with the controls (Tables S5 and S6).

To obtain a global view of the biological processes, molecular function, and cellular components represented by these proteins a gene ontology analysis was performed and protein-protein interaction schemes were constructed. Most of the proteins under-expressed in the mutant LVF were involved in intracellular signaling, ocular function, ocular tissue repair and homeostasis, cell structure, growth and metabolism and included members of the cytochrome P450 and proteasome systems, the neurotrophin pathway, as well as proteins involved in photo-transduction, glycolysis, the function of the citric acid cycle (Figure 3, Table 2) and several crystallins (Figure 4A-B). It is of interest that ARF4, a protein thought to

be important for the trafficking of the light receptor rhodopsin [33] as well as of LRP2 [34] (Figure 4C) was strongly decreased in the mutant LVF.

The proteins over-expressed in the mutant LVF included transport proteins (afamin, albumin, apolipoprotein A-IV, apolipoprotein E, clusterin, ceruloplasmin, corticosteroid-binding globulin, retinol-binding protein, selenoprotein, transcobalamin, transferrin, transthyretin, vitamin-D binding protein); acute-phase response proteins (a-1-antitrypsin, a-2-HS-glycoprotein, angiotensinogen, chitinase 3-like 1); proteins involved in cell growth, maintenance and metabolism (carbonic anhydrase I, gelsolin, liver carboxypeptidase N); complement system proteins, immunoglobulins (illustrated in Figure 5), cell adhesion proteins (zinc-alpha-2-glycoprotein), fibrinolytic and clotting system proteins (anti-thrombin-III, alpha-2-antiplasmin, alpha-2 macroglobulin, plasminogen, prothrombin, kininogen, kallikrein). Among them at least 30, including alpha-amylase, albumin, transferrin, retinol-binding protein, selenoprotein, transcobalamin, clusterin, transthyrtein, angiotensinogen, carbonic anhydrase 1, alpha-2 macroglobulin, alpha-2 antiplasmin and anti-thrombin-III are known LRP2 ligands (Figure 6 and [35]).

Remarkably most of the proteins overexpressed in the mutant LVF, including the LRP2 ligands may originate from the serum, suggesting impaired function of the blood-ocular barriers, tissues that normally express LRP2. We therefore first investigated the structure of the CE and RPE in control and mutant eyes using transmission electron (TEM) and confocal microscopy.

3.3. Morphological modifications of the LRP2-deficient cells

Two barriers have been described in the eye: the blood-retinal (BRB) and the blood-aqueous barrier (BAB). The BRB is particularly restrictive and regulates ion, protein and

water flux into and out of the retina. It has an inner component provided by the inter endothelial tight junctions (TJs) of the intra-retinal vasculature and an outer one provided by TJs between the RPE cells [36–38]. TJs between the non-pigmented layer of the CE as well as the endothelial cells of the iris vasculature provide the blood-aqueous barrier [39,40].

TEM of control and *Lrp2*-deficient ciliary processes did not reveal any difference in the formation and structure of the TJs and adherent junctions (AJ) at the level of the non-pigmented ciliary epithelial cells (Fig. 7A-B). Furthermore the expression of occludin, a membrane protein essential for both the establishment and maintenance of TJs, appeared preserved both in the mutant ciliary body vasculature and between the non-pigmented cells of the *Lrp2*-deficient eye (Fig. 7C-D).

TEM analysis of normal RPE cells was as previously described [41] (Fig. 7E-F). The RPE cells carried extremely long apical microvilli (20–30 μm) surrounding the outer rod segments (Fig. 7E). The basal plasma membrane of RPE cells displayed highly convoluted micro-infolds and interacted with the underlying choroidal capillaries through the Bruch's membrane (Fig. 7E). TJs followed by AJs were easily observed in the control RPE (Fig. 7F). In the mutants the outer rod segments were absent and the morphology of the apical domain of RPE cells was dramatically modified; the apical microvilli were lost and replaced by short, convoluted, less ordered structures (Fig. 7G-H) suggestive of apical dedifferentiation. In addition the AJs between adjacent RPE cells appeared shorter compared with the controls and the TJs were smaller or even absent (Fig. 7I-J) suggesting that the barrier function of the mutant RPE cells might be compromised.

Confocal microscopy and western blot analyses showed ectopic, strong expression of alpha-smooth muscle actin (Fig. 7K-L) in the mutant RPE, increased expression of the mesenchymal proteins collagen type 1 and decreased expression of zonula occludens 1 (ZO-

1), a protein associated with both TJs and AJs (Fig. 7M). These protein modifications are consistent with the TEM observations and apical dedifferentiation of the LRP2-deficient RPE cells [42], and this was further confirmed by the increased expression of phosphorylated Erk1/2 (Fig. 7M), a signaling marker activated in RPE cells upon initiation of trans-differentiation to a mesenchymal-like morphology [43].

Endocytosis as well as lysosomal degradation of material derived through the autophagic or phagocytotic pathways are essential RPE functions and their impairment triggers retinopathy [44]. In this context it is interesting to note that the loss of LRP2 function in the zebrafish pronephros has previously been associated with abrogation of endocytosis due to the impaired formation of the endocytic apparatus [45]. Conversely inactivation of the lysosomal integral protein-2 (LIMP2) impairs the lysosomal pathway in the marginal cells of stria vascularis as well as membrane expression of Lrp2, a defect preceding overt hearing loss in the LIMP2 null mutants [46]. We therefore analyzed the expression of the classical early endocytic and lysosomal markers EEA1, cathepsin D and LIMP2 in control and LRP2-deficient RPE extracts. EEA1 levels were decreased in the mutants suggesting that the early steps of endocytosis may be perturbed (Fig. 7N). With respect to cathepsin D two bands were detected in the control RPE; one of around 52 kDa corresponding with the immature form of the protein, and a second one of around 28 kDa corresponding with a mature one [47]. It is of interest that the expression of mature cathepsin D was almost completely abolished in the mutants specifically in the RPE (Fig. 7N). Furthermore the expression of LIMP2, a protein required for the biogenesis and maintenance of lysosomes [48] was strongly reduced in the mutants (Fig. 7N). To directly test *in vivo* protein endocytosis by the RPE we analyzed the uptake of Alexa 488-labeled albumin, an LRP2 ligand and of Alexa 488-labeled transferrin, a protein that may be internalized by both LRP2 and the transferrin receptor. After intravenous eye injection of P60 control mice a definite albumin or transferrin uptake and localization in

large vacuoles/lysosomes was observed in the RPE (Fig. 7O) and as previously shown [49] at the renal proximal convoluted tubule. Whereas the renal reabsorption was not affected in $Lrp2^{FoxG1.cre\text{-}KO}$ mutants, no albumin- or transferrin-containing vacuoles were detectable in the mutant RPE (Fig. 7P) strongly suggesting that Lrp2 function is necessary for the formation of the RPE endocytic apparatus.

Impaired endocytosis, loss of lysosomes and decreased LRP2 expression were recently observed in the visceral endoderm (VE) of the Arf4 null mice [34] that die at mid-gestation most likely due to the impairment of the absorptive VE functions. Western blot analysis showed that ARF4 was readily detected in the retina (Fig. 7Q and [33]) as well as the RPE of control mice. Furthermore ARF4 and LRP2 were co-immunoprecipitated (Fig. 7R) suggesting that these proteins may physically interact. However, in the LRP2-deficient RPE ARF4 was hardly detectable (Fig. 7Q) suggesting that the lack of LRP2 perturbs not only the endocytic process but possibly also protein trafficking in the mutant RPE. Supporting this idea the expression of the recycling endosome marker Rab11, a known ARF4 partner (Fig. 7Q) required for LRP2 recycling [50] was strongly decreased in the mutants. Although the analysis of the phagocytic function of the LRP2-deficient RPE cells is beyond the scope of this work, the above results support the idea that impaired formation of the RPE barrier and endocytic apparatus most likely contribute to the vitreal modifications and the severe retinopathy observed in the LRP2-deficient eyes.

4. Discussion

We here analyzed the impact of Lrp2 ablation on the composition of the vitreous and the structure and function of RPE. We identified several ionic and protein modifications that may, at least partly reflect defective metabolism in the ocular tissues that surround the vitreal cavity as well as signs of RPE cell dedifferentiation. We showed that LRP2 ablation impairs protein endocytosis in the RPE and that the expression of several factors involved in the formation of the endocytic apparatus was strongly reduced. We proposed that these morphological and functional RPE alterations contribute to the progression of the HM and associated retinopathy.

4.1. Vitreous liquefaction and ionic modifications of the LVF in HM

Using the chick model several groups showed that in form deprivation (FD) myopia the axial elongation of the myopic globe is directly related to an increase of the liquid vitreous volume [7,16,51]. Our results also show that the increase in vitreous chamber depth is accompanied by an excessive increase of the LVF supporting its contribution in abnormal eye enlargement. The presence of liquid vitreous may result from vitreous gel liquefaction, i.e. the enzymatic digestion of the vitreous gel known to physiologically occur in aging vitreous [52–54]. In the LRP2-deficient eyes however, the mass of the vitreous gel fraction was not apparently modified arguing against a major contribution of this process in the formation of LVF.

Electrolyte analysis of the liquid vitreous in FD eyes showed an increased abundance in chloride and decreased concentrations of potassium and phosphorus [16]. In our genetic model of HM the abundance in potassium was also significantly decreased in the LVF, however the concentrations of chloride and phosphorus were decreased or increased respectively. Despite the discrepancy in phosphorus abundance, most likely due to differences

in animal models and/or experimental designs, it is clear that the electrolytic balance of the liquid vitreous is altered in the highly myopic eyes and that the abundance of potassium, essential for the regulation of retinal cell membrane potential, may be one of the elements involved in the induction/maintenance of the myopic eye growth. Furthermore the significantly increased concentrations of phosphorus and calcium in the myopic LVF may eventually lead to intraocular calcification and/or reflect an inflammatory status, a condition known to be associated with HM [55]. Impaired electrolyte composition of the vitreous may at least partly be explained by the dysfunction of Müller cells, one of the cell types involved in transretinal ionic and fluid transport [56]. This hypothesis is indeed supported by our previous results [3] showing an intense glial fibrillary acidic protein staining of the Müller cells in the mutant retinas and extensive gliosis as soon as post-natal day 10 (P10).

4.2. Protein modifications of the LVF in HM

4.2.1. Various crystallins and proteins involved in photo-transduction and amacrine-cell function are significantly decreased in the LVF of the *Lrp2*-deficient eyes.

Crystallins were originally described as lens-specific structural proteins essential for its refractive properties [57] but their wider expression in ocular and extra-ocular tissues is established [58]. Alpha crystallins belong to the small heat-shock protein family, regulate apoptosis and are thought to be involved in the pathogenesis of HM-induced cataract [59]. The function of beta- and gamma-crystallins is less clear but these proteins are also involved in apoptosis regulation as well as in retinal axon growth regeneration [58]. Recently decreased levels of beta-crystallin S, beta-crystallin B2 and gamma-crystallin C were reported in the aqueous humor of HM patients [60]. The same crystallins as well as of four additional family members were also dramatically reduced in the LVF of LRP-2-deficient eyes. This observation is well correlated with the continuous and increased apoptosis observed in the

retina of the LRP2-deficient eyes [3] and suggests that downregulation of these proteins contributes to the pathogenesis of the myopic retinopathy.

In addition, the abundance of recoverin, phosducin, S-arrestin, interphotoreceptor-retinoid binding protein, retinoschisin, calbindin, calretinin and calcium-calmodulin dependent protein kinase II was dramatically decreased in the mutant LVF. These proteins are produced by retinal photoreceptors, amacrine, bipolar and/or ganglion cells and required for photoreceptor differentiation and/or function. The reduced expression of these proteins is consistent with the degeneration of the above retinal cell types observed in the LRP2-deficient eyes [3] as well as the absence of rod outer segments described here. It may reflect the progression of the disease and/or be associated with the myopic eye growth. The three-fold decreased expression of the amyloid beta precursor-like protein 2, modulator of amacrine cell function, and recently identified myopia-susceptibility gene [61] further supports this hypothesis.

Finally, retinaldehyde dehydrogenase 2 (RALDH2), an enzyme essential for the synthesis of all-trans-retinoic acid (RA), strongly expressed in the human RPE [62] and essential in visually-guided normal and myopic eye growth [63], was not detectable in the LVF of the LRP2-deficient eyes. Our finding is in full agreement with the de-differentiation of the LRP2-deficient cells, the essential role of RALDH2 in myopic eye growth and may suggest a direct and/or indirect role of LRP2 in RA homeostasis in the eye.

4.2.2. Various Lrp2 ligands as well as proteins of the complement, coagulation and immune systems are significantly increased in the LVF of the Lrp2-deficient eyes

The level of 74 proteins was two- to 14-fold higher in the mutant LVF. LRP2 is clearly associated with the uptake and cellular handling of numerous of these proteins in neuronal and non-neuronal tissues [35,64]. Furthermore the LRP2-ligands albumin,

transthyrretin and vitamin-D binding protein were previously reported to be upregulated in the ocular fluids of HM patients [65,66]. Although the specific function of these proteins in the ocular tissues remains unclear the above observations support their significance as potential myopia biomarkers or pathogenic factors and may indirectly involve LRP2 in the regulation of eye growth.

The levels of components of the complement, kinin-kallikrein and immune systems, or several inflammation-associated proteins such as alpha1-antitrypsin and transferrin were significantly increased in the mutant LVF. These modifications are consistent with the presence of an inflammatory microenvironment in the myopic LRP2-deficient eye and in agreement with the idea that HM is an inflammation-related disease [55].

Thrombin is a multifunctional protein with both proteinase and growth-factor like activities. Thrombin activity is physiologically detected in the vitreous liquid [67] where it may be needed to avoid bleeding events. Increased thrombin activity was previously reported in patients with rhegmatogenous retinal detachment [68]. The expression of factors of the thrombin pathway including alpha-2 antiplasmin, alpha-2 macroglobulin, antithrombin III and plasminogen was significantly increased in the LRP2-deficient LVF suggesting an association with the evolution of the disease.

4.3. Morphological and functional defects of the LRP2-deficient RPE cells may contribute to the vitreous modifications and myopic retinopathy

A significantly higher abundance of several proteins of the complement, coagulation or immune systems was found in the vitreous of patients with diabetic retinopathy, age-related macular degeneration or proliferative vitreoretinopathy [28,69–71]. In these cases however the increased vitreal protein concentration was most probably linked to a systemic dysregulation and an intraocular leakage of serum proteins due to the breakdown of the ocular

barriers [70,72]. The modifications that we observe in the LRP2-deficient LVF are unlikely to be systemic as indicated by the similar ionic composition of the serum in control and mutant mice as well as the physiological levels of the major serum components albumin and transferrin in the mutants.

Ultrastructural analysis of the outer BRB forming RPE cells showed that the apical morphology of the RPE cells was severely affected in the mutants. Furthermore, the formation of the TJs, crucial for the epithelial barrier function was compromised and the mutant RPE cells abnormally expressed mesenchymal markers including aSMA, collagen and fibronectin, well described signs of RPE fibrosis [43,73] and often observed after rhegmatogenous retinal detachment. These observations suggested that RPE cell dysfunction, the most likely ensuing impaired transretinal and ionic fluid transport [56] and disruption of the BRB barriers may be associated events and contribute to the mutant LVF modifications. They furthermore suggested that the LRP2-deficient RPE cells might be less protected against LVF components with pathogenic potential.

Defective serum protein endocytosis and apical dedifferentiation of the epithelial proximal tubule cells has previously been associated with loss of LRP2 in the cystotic mouse kidney [74]. In line with a central role of LRP2 in protein uptake in the RPE, its inactivation interfered with endocytic uptake of albumin and transferrin specifically in this tissue demonstrating the conservation of this pathway in the ocular tissues. Moreover the mutant RPE lacks the lysosomal structures normally present in the control RPE and the expression of proteins involved in various steps of the endocytic process, including EEA1, Rab11, cathepsin D and LIMP2, is strongly reduced. These findings might reflect a preponderant implication of LRP2 in protein endocytosis in the RPE. Alternatively LRP2 might be directly required for the establishment of an endocytic apparatus in the RPE, a hypothesis compatible with the lack of detectable endocytic structures in the kidney of the LRP2 null mutants [75]. The absence of

LRP2 activity has previously been observed in mice lacking ARF4 [34], a protein thought to play a key role in transmembrane protein sorting and to be possibly involved in human diseases such as retinal degeneration. In line with a potential implication of LRP2 in the formation of a proper endocytic machinery, ARF4 interacts with LRP2 in the control RPE whereas its expression is strongly reduced in the mutant. Disruption of lysosomal formation affects a multitude of cellular processes in the RPE, including the phagocytosis of photoreceptor outer segments tips and is thought to contribute to chronic retinal degenerations [44,76]. We propose that the myopic retinopathy observed in the LRP2 mutants [3] is directly associated with defective lysosomal formation in the RPE.

In sum our work provides the first differential analysis of the ionic and protein content of the myopic vitreous, uncovers novel potential biomarkers of HM and identifies the RPE cell layer as a pathogenic target/actor of HM associated pathologies. It strongly suggests that LRP2 may be an essential component of the protein network that regulates eye growth and provides a framework for detailed approaches to dissect the molecular components involved in the development and progression of HM.

Funding provided by RK: Institut National sur la Recherche Médicale ANR-10-LABX-65, ANR-11-IDEX-004-02, and Sanofi-Ophtalmology. Sanofi provided support but did not have any additional role in the study design, data collection and analysis, decision to publish, or preparation of the manuscript.

Table 1. Ionic composition of control and mutant liquid vitreous fraction (LVF) at P90. The number of eyes (n) used for one analysis is indicated. The number of analysis (m) for each condition is indicated.

	Plasma 3 mths		LVF 3 mths	
	Control (*n* = 1) (m = 5)	Mutant (*n* = 1) (m = 4)	Control (n = 30) (m = 3)	Mutant (n = 6) (m = 3)
Sodium mmol/L	147.2 ± 1.6	148.5 ± 1	167 ± 1.2	154 ± 1.5
Potassium mmol/L	6.1 ± 0.8	5.7 ± 0.3	17 ± 0.9	7.6 ± 0.5
Chloride mmol/L	111.2 ± 0.2	114.4 ± 1.3	144 ± 1.2	128 ± 1.3
Lactate mmol /l	4.5 ± 0.6	4.7 ± 0.7	9.5 ± 0.6	10.2 ± 0.6
Glucose mmol/l	4.8 ± 0.2	5.2 ± 0.2	6.23 ± 0.2	6.05 ± 0.2
Calcium mmol/L	2.31 ± 0.04	2.31 ± 0.05	0.3 ± 0.05	0.82 ± 0.02
Phosphorus mmol/l	2.01 ± 0.06	2.07 ± 0.07	1 ± 0.05	2.41 ± 0.01
Iron μmol/L	25.0 ± 2.1	27.1 ± 3	~0	2.2 ± 0.05
Antioxidant status mmol/l	n.d.	n.d.	0.12 ± 0.01	0.067 ± 0.01
Osmolality mosm/l	287.3	289.3	346.1	307.8
Total protein g/L	45.2 ± 1.4	44.1 ± 1.1	0.3 ± 0.007	0.9 ± 0.009
Albumin g/L	26.8 ± 0.9	28.0 ± 0.5	0.04	0.23
Transferrin g/L	0.85 ± 0.09	0.81 ± 0.07	~0	0.03

Values are means ± SEM of plasma clinical chemistry results. n.d.: not determined.

Table 2. Pathways down-regulated in the mutant vitreous fluid.

The table lists the number of proteins (N) participating in each pathway, the associated *p*-value and the mean fold change of protein abundance.

Pathways	N	*p*-value	ratio
Metabolism			
Glycerolipid and glycolysis	21	$1.75\ 10^{-20}$	3.67
Citric acid cycle	9	$3.67\ 10^{-8}$	3.97
Regulation			
Cytochrome P-450	11	$2.04\ 10^{-7}$	3.23
Phototransduction	6	$3.73\ 10^{-5}$	529
Proteasome	10	$4.37\ 10^{-8}$	13.5
Neurotrophin	10	$2.66\ 10^{-4}$	5.58
Protein processing	17	$5.99\ 10^{-8}$	8.99
Actin cytoskeleton	17	$2.03\ 10^{-6}$	4.3

REFERENCES

[1] S. Kantarci, L. Al-Gazali, R.S. Hill, D. Donnai, G.C.M. Black, E. Bieth, N. Chassaing, D. Lacombe, K. Devriendt, A. Teebi, M. Loscertales, C. Robson, T. Liu, D.T. MacLaughlin, K.M. Noonan, M.K. Russell, C.A. Walsh, P.K. Donahoe, B.R. Pober, Mutations in LRP2, which encodes the multiligand receptor megalin, cause Donnai-Barrow and facio-oculo-acoustico-renal syndromes, Nat. Genet. 39 (2007) 957–959. doi:10.1038/ng2063.

[2] B.R. Pober, M. Longoni, K.M. Noonan, A review of Donnai-Barrow and facio-oculo-acoustico-renal (DB/FOAR) syndrome: clinical features and differential diagnosis, Birt. Defects Res. A. Clin. Mol. Teratol. 85 (2009) 76–81. doi:10.1002/bdra.20534.

[3] O. Cases, A. Joseph, A. Obry, M.D. Santin, S. Ben-Yacoub, M. Pâques, S. Amsellem-Levera, A. Bribian, M. Simonutti, S. Augustin, T. Debeir, J.A. Sahel, A. Christ, F. de Castro, S. Lehéricy, P. Cosette, R. Kozyraki, Foxg1-Cre Mediated Lrp2 Inactivation in the Developing Mouse Neural Retina, Ciliary and Retinal Pigment Epithelia Models Congenital High Myopia, PloS One. 10 (2015) e0129518. doi:10.1371/journal.pone.0129518.

[4] P.-B. Ouyang, X.-C. Duan, X.-H. Zhu, Diagnosis and treatment of myopic traction maculopathy, Int. J. Ophthalmol. 5 (2012) 754–758. doi:10.3980/j.issn.2222-3959.2012.06.19.

[5] I.G. Morgan, K. Ohno-Matsui, S.-M. Saw, Myopia, Lancet. 379 (2012) 1739–1748. doi:10.1016/S0140-6736(12)60272-4.

[6] J.B. Jonas, L. Xu, Histological changes of high axial myopia, Eye Lond. Engl. 28 (2014) 113–117. doi:10.1038/eye.2013.223.

[7] M.M. Le Goff, P.N. Bishop, Adult vitreous structure and postnatal changes, Eye Lond. Engl. 22 (2008) 1214–1222. doi:10.1038/eye.2008.21.

[8] J.P. Monteiro, F.M. Santos, A.S. Rocha, J.P. Castro-de-Sousa, J.A. Queiroz, L.A. Passarinha, C.T. Tomaz, Vitreous humor in the pathologic scope: insights from proteomic approaches, Proteomics Clin. Appl. 9 (2015) 187–202. doi:10.1002/prca.201400133.

[9] J. Sebag, Ageing of the vitreous, Eye Lond. Engl. 1 (Pt 2) (1987) 254–262. doi:10.1038/eye.1987.45.

[10] Y.-B. Shui, N.M. Holekamp, B.C. Kramer, J.R. Crowley, M.A. Wilkins, F. Chu, P.E. Malone, S.J. Mangers, J.H. Hou, C.J. Siegfried, D.C. Beebe, The gel state of the vitreous and ascorbate-dependent oxygen consumption: relationship to the etiology of nuclear cataracts, Arch. Ophthalmol. Chic. Ill 1960. 127 (2009) 475–482. doi:10.1001/archophthalmol.2008.621.

[11] H. Watanabe, K. Kohzaki, H. Kubo, K. Okano, A. Watanabe, H. Tsuneoka, [Stickler syndrome with rhegmatogenous retinal detachment], Nippon Ganka Gakkai Zasshi. 114 (2010) 454–458.

[12] N.M. Holekamp, G.J. Harocopos, Y.-B. Shui, D.C. Beebe, Myopia and axial length contribute to vitreous liquefaction and nuclear cataract, Arch. Ophthalmol. Chic. Ill 1960. 126 (2008) 744; author reply 744. doi:10.1001/archopht.126.5.744-a.

[13] S. Satofuka, Y. Imamura, S. Ishida, Y. Ozawa, K. Tsubota, M. Inoue, Rhegmatogenous retinal detachment associated with primary congenital glaucoma, Int. Ophthalmol. 28 (2008) 369–371. doi:10.1007/s10792-007-9142-x.

[14] T.Y.Y. Lai, D.S.P. Fan, W.W.K. Lai, D.S.C. Lam, Peripheral and posterior pole retinal lesions in association with high myopia: a cross-sectional community-based study in Hong Kong, Eye Lond. Engl. 22 (2008) 209–213. doi:10.1038/sj.eye.6702573.

[15] E.R. Berman, I.C. Michaelson, THE CHEMICAL COMPOSITION OF THE HUMAN VITREOUS BODY AS RELATED TO AGE AND MYOPIA, Exp. Eye Res. 3 (1964) 9–15.

[16] Y. Seko, H. Shimokawa, J. Pang, T. Tokoro, Disturbance of electrolyte balance in vitreous of chicks with form-deprivation myopia, Jpn. J. Ophthalmol. 44 (2000) 15–19.

[17] R.L. Seltner, J.G. Sivak, A role for the vitreous humor in experimentally-induced myopia, Am. J. Optom. Physiol. Opt. 64 (1987) 953–957.

[18] A. Hosaka, Permeability of the blood-retinal barrier in myopia. An analysis employing vitreous fluorophotometry and computer simulation, Acta Ophthalmol. Suppl. 185 (1988) 95–99.

[19] A. Yoshida, S. Ishiko, M. Kojima, Inward and outward permeability of the blood-retinal barrier in experimental myopia, Graefes Arch. Clin. Exp. Ophthalmol. Albrecht Von Graefes Arch. Für Klin. Exp. Ophthalmol. 234 Suppl 1 (1996) S239-242.

[20] N. Kitaya, S. Ishiko, T. Abiko, F. Mori, H. Kagokawa, M. Kojima, K. Saito, A. Yoshida, Changes in blood-retinal barrier permeability in form deprivation myopia in tree shrews, Vision Res. 40 (2000) 2369–2377.

[21] W. Meng, J. Butterworth, F. Malecaze, P. Calvas, Axial length of myopia: a review of current research, Ophthalmol. J. Int. Ophtalmol. Int. J. Ophthalmol. Z. Für Augenheilkd. 225 (2011) 127–134. doi:10.1159/000317072.

[22] G.J. Harocopos, Y.-B. Shui, M. McKinnon, N.M. Holekamp, M.O. Gordon, D.C. Beebe, Importance of vitreous liquefaction in age-related cataract, Invest. Ophthalmol. Vis. Sci. 45 (2004) 77–85.

[23] M.-F. Champy, M. Selloum, V. Zeitler, C. Caradec, B. Jung, S. Rousseau, L. Pouilly, T. Sorg, J. Auwerx, Genetic background determines metabolic phenotypes in the mouse,

Mamm. Genome Off. J. Int. Mamm. Genome Soc. 19 (2008) 318–331. doi:10.1007/s00335-008-9107-z.

[24] S. Lussignoli, M. Fraccaroli, G. Andrioli, G. Brocco, P. Bellavite, A microplate-based colorimetric assay of the total peroxyl radical trapping capability of human plasma, Anal. Biochem. 269 (1999) 38–44. doi:10.1006/abio.1999.4010.

[25] M. Kampa, A. Nistikaki, V. Tsaousis, N. Maliaraki, G. Notas, E. Castanas, A new automated method for the determination of the Total Antioxidant Capacity (TAC) of human plasma, based on the crocin bleaching assay, BMC Clin. Pathol. 2 (2002) 3.

[26] C.W. Wu, J.L. Sauter, P.K. Johnson, C.-D. Chen, T.W. Olsen, Identification and localization of major soluble vitreous proteins in human ocular tissue, Am. J. Ophthalmol. 137 (2004) 655–661. doi:10.1016/j.ajo.2003.11.009.

[27] J.M. Skeie, V.B. Mahajan, Proteomic interactions in the mouse vitreous-retina complex, PloS One. 8 (2013) e82140. doi:10.1371/journal.pone.0082140.

[28] M.J. Koss, J. Hoffmann, N. Nguyen, M. Pfister, H. Mischak, W. Mullen, H. Husi, R. Rejdak, F. Koch, J. Jankowski, K. Krueger, T. Bertelmann, J. Klein, J.P. Schanstra, J. Siwy, Proteomics of vitreous humor of patients with exudative age-related macular degeneration, PloS One. 9 (2014) e96895. doi:10.1371/journal.pone.0096895.

[29] K.R. Murthy, R. Goel, Y. Subbannayya, H.K. Jacob, P.R. Murthy, S.S. Manda, A.H. Patil, R. Sharma, N.A. Sahasrabuddhe, A. Parashar, B.G. Nair, V. Krishna, T.K. Prasad, H. Gowda, A. Pandey, Proteomic analysis of human vitreous humor, Clin. Proteomics. 11 (2014) 29. doi:10.1186/1559-0275-11-29.

[30] B.-B. Gao, A. Clermont, S. Rook, S.J. Fonda, V.J. Srinivasan, M. Wojtkowski, J.G. Fujimoto, R.L. Avery, P.G. Arrigg, S.-E. Bursell, L.P. Aiello, E.P. Feener, Extracellular

carbonic anhydrase mediates hemorrhagic retinal and cerebral vascular permeability through prekallikrein activation, Nat. Med. 13 (2007) 181–188. doi:10.1038/nm1534.

[31] J.M. Skeie, C.N. Roybal, V.B. Mahajan, Proteomic insight into the molecular function of the vitreous, PloS One. 10 (2015) e0127567. doi:10.1371/journal.pone.0127567.

[32] P. Liang, T.H. MacRae, Molecular chaperones and the cytoskeleton, J. Cell Sci. 110 (Pt 13) (1997) 1431–1440.

[33] D. Deretic, J. Wang, Molecular assemblies that control rhodopsin transport to the cilia, Vision Res. 75 (2012) 5–10. doi:10.1016/j.visres.2012.07.015.

[34] J.A. Follit, J.T. San Agustin, J.A. Jonassen, T. Huang, J.A. Rivera-Perez, K.D. Tremblay, G.J. Pazour, Arf4 Is Required for Mammalian Development but Dispensable for Ciliary Assembly, PLoS Genet. 10 (2014) e1004170. doi:10.1371/journal.pgen.1004170.

[35] R. Kozyraki, F. Gofflot, Multiligand endocytosis and congenital defects: roles of cubilin, megalin and amnionless, Curr. Pharm. Des. 13 (2007) 3038–3046.

[36] J. Cunha-Vaz, R. Bernardes, C. Lobo, Blood-retinal barrier, Eur. J. Ophthalmol. 21 Suppl 6 (2011) S3-9. doi:10.5301/EJO.2010.6049.

[37] L.J. Rizzolo, Barrier properties of cultured retinal pigment epithelium, Exp. Eye Res. 126 (2014) 16–26. doi:10.1016/j.exer.2013.12.018.

[38] F. Willermain, S. Libert, E. Motulsky, D. Salik, L. Caspers, J. Perret, C. Delporte, Origins and consequences of hyperosmolar stress in retinal pigmented epithelial cells, Front. Physiol. 5 (2014) 199. doi:10.3389/fphys.2014.00199.

[39] T.F. Freddo, A contemporary concept of the blood-aqueous barrier, Prog. Retin. Eye Res. 32 (2013) 181–195. doi:10.1016/j.preteyeres.2012.10.004.

[40] M. Coca-Prados, The blood-aqueous barrier in health and disease, J. Glaucoma. 23 (2014) S36-38. doi:10.1097/IJG.0000000000000107.

[41] G.L. Lehmann, I. Benedicto, N.J. Philp, E. Rodriguez-Boulan, Plasma membrane protein polarity and trafficking in RPE cells: past, present and future, Exp. Eye Res. 126 (2014) 5–15. doi:10.1016/j.exer.2014.04.021.

[42] J. Bastiaans, J.C. van Meurs, C. van Holten-Neelen, N.M.A. Nagtzaam, P.M. van Hagen, R.C. Chambers, H. Hooijkaas, W.A. Dik, Thrombin induces epithelial-mesenchymal transition and collagen production by retinal pigment epithelial cells via autocrine PDGF-receptor signaling, Invest. Ophthalmol. Vis. Sci. 54 (2013) 8306–8314. doi:10.1167/iovs.13-12383.

[43] K. Kimura, T. Orita, Y. Liu, Y. Yang, K. Tokuda, T. Kurakazu, T. Noda, R. Yanai, N. Morishige, A. Takeda, T. Ishibashi, K.-H. Sonoda, Attenuation of EMT in RPE cells and subretinal fibrosis by an RAR-γ agonist, J. Mol. Med. Berl. Ger. 93 (2015) 749–758. doi:10.1007/s00109-015-1289-8.

[44] S. Guha, E.E. Coffey, W. Lu, J.C. Lim, J.M. Beckel, A.M. Laties, K. Boesze-Battaglia, C.H. Mitchell, Approaches for detecting lysosomal alkalinization and impaired degradation in fresh and cultured RPE cells: evidence for a role in retinal degenerations, Exp. Eye Res. 126 (2014) 68–76. doi:10.1016/j.exer.2014.05.013.

[45] U. Anzenberger, N. Bit-Avragim, S. Rohr, F. Rudolph, B. Dehmel, T.E. Willnow, S. Abdelilah-Seyfried, Elucidation of megalin/LRP2-dependent endocytic transport processes in the larval zebrafish pronephros, J. Cell Sci. 119 (2006) 2127–2137. doi:10.1242/jcs.02954.

[46] M. Knipper, C. Claussen, L. Rüttiger, U. Zimmermann, R. Lüllmann-Rauch, E.-L. Eskelinen, J. Schröder, M. Schwake, P. Saftig, Deafness in LIMP2-deficient mice due to early loss of the potassium channel KCNQ1/KCNE1 in marginal cells of the stria vascularis, J. Physiol. 576 (2006) 73–86. doi:10.1113/jphysiol.2006.116889.

[47] A.H. Erickson, G.E. Conner, G. Blobel, Biosynthesis of a lysosomal enzyme. Partial structure of two transient and functionally distinct NH2-terminal sequences in cathepsin D, J. Biol. Chem. 256 (1981) 11224–11231.

[48] A. Gonzalez, M. Valeiras, E. Sidransky, N. Tayebi, Lysosomal integral membrane protein-2: a new player in lysosome-related pathology, Mol. Genet. Metab. 111 (2014) 84–91. doi:10.1016/j.ymgme.2013.12.005.

[49] S. Amsellem, J. Gburek, G. Hamard, R. Nielsen, T.E. Willnow, O. Devuyst, E. Nexo, P.J. Verroust, E.I. Christensen, R. Kozyraki, Cubilin is essential for albumin reabsorption in the renal proximal tubule, J. Am. Soc. Nephrol. JASN. 21 (2010) 1859–1867. doi:10.1681/ASN.2010050492.

[50] A.E. Perez Bay, R. Schreiner, I. Benedicto, M. Paz Marzolo, J. Banfelder, A.M. Weinstein, E.J. Rodriguez-Boulan, The fast-recycling receptor Megalin defines the apical recycling pathway of epithelial cells, Nat. Commun. 7 (2016) 11550. doi:10.1038/ncomms11550.

[51] W. Halfter, U. Winzen, P.N. Bishop, A. Eller, Regulation of eye size by the retinal basement membrane and vitreous body, Invest. Ophthalmol. Vis. Sci. 47 (2006) 3586–3594. doi:10.1167/iovs.05-1480.

[52] L.I. Los, R.J. van der Worp, M.J.A. van Luyn, J.M.M. Hooymans, Age-related liquefaction of the human vitreous body: LM and TEM evaluation of the role of proteoglycans and collagen, Invest. Ophthalmol. Vis. Sci. 44 (2003) 2828–2833.

[53] M. van Deemter, H.H. Pas, R. Kuijer, R.J. van der Worp, J.M.M. Hooymans, L.I. Los, Enzymatic breakdown of type II collagen in the human vitreous, Invest. Ophthalmol. Vis. Sci. 50 (2009) 4552–4560. doi:10.1167/iovs.08-3125.

[54] M. van Deemter, R. Kuijer, H. Harm Pas, R. Jacoba van der Worp, J.M.M. Hooymans, L.I. Los, Trypsin-mediated enzymatic degradation of type II collagen in the human vitreous, Mol. Vis. 19 (2013) 1591–1599.

[55] C.P. Herbort, M. Papadia, P. Neri, Myopia and inflammation, J. Ophthalmic Vis. Res. 6 (2011) 270–283.

[56] A. Bringmann, T. Pannicke, J. Grosche, M. Francke, P. Wiedemann, S.N. Skatchkov, N.N. Osborne, A. Reichenbach, Müller cells in the healthy and diseased retina, Prog. Retin. Eye Res. 25 (2006) 397–424. doi:10.1016/j.preteyeres.2006.05.003.

[57] J. Graw, Genetics of crystallins: cataract and beyond, Exp. Eye Res. 88 (2009) 173–189. doi:10.1016/j.exer.2008.10.011.

[58] S. Thanos, M.R.R. Böhm, M. Meyer zu Hörste, V. Prokosch-Willing, M. Hennig, D. Bauer, A. Heiligenhaus, Role of crystallins in ocular neuroprotection and axonal regeneration, Prog. Retin. Eye Res. 42 (2014) 145–161. doi:10.1016/j.preteyeres.2014.06.004.

[59] X.-J. Zhu, P. Zhou, K.-K. Zhang, J. Yang, Y. Luo, Y. Lu, Epigenetic regulation of αA-crystallin in high myopia-induced dark nuclear cataract, PloS One. 8 (2013) e81900. doi:10.1371/journal.pone.0081900.

[60] Y. Ji, X. Rong, H. Ye, K. Zhang, Y. Lu, Proteomic analysis of aqueous humor proteins associated with cataract development, Clin. Biochem. 48 (2015) 1304–1309. doi:10.1016/j.clinbiochem.2015.08.006.

[61] A.V. Tkatchenko, T.V. Tkatchenko, J.A. Guggenheim, V.J.M. Verhoeven, P.G. Hysi, R. Wojciechowski, P.K. Singh, A. Kumar, G. Thinakaran, Consortium for Refractive Error and Myopia (CREAM), C. Williams, APLP2 Regulates Refractive Error and Myopia Development in Mice and Humans, PLoS Genet. 11 (2015) e1005432. doi:10.1371/journal.pgen.1005432.

[62] A.R. Harper, A.F. Wiechmann, G. Moiseyev, J.-X. Ma, J.A. Summers, Identification of active retinaldehyde dehydrogenase isoforms in the postnatal human eye, PloS One. 10 (2015) e0122008. doi:10.1371/journal.pone.0122008.

[63] J.A.S. Rada, L.R. Hollaway, W. Lam, N. Li, J.L. Napoli, Identification of RALDH2 as a visually regulated retinoic acid synthesizing enzyme in the chick choroid, Invest. Ophthalmol. Vis. Sci. 53 (2012) 1649–1662. doi:10.1167/iovs.11-8444.

[64] C.E. Fleming, F.M. Mar, F. Franquinho, M.J. Saraiva, M.M. Sousa, Transthyretin internalization by sensory neurons is megalin mediated and necessary for its neuritogenic activity, J. Neurosci. Off. J. Soc. Neurosci. 29 (2009) 3220–3232. doi:10.1523/JNEUROSCI.6012-08.2009.

[65] X. Duan, Q. Lu, P. Xue, H. Zhang, Z. Dong, F. Yang, N. Wang, Proteomic analysis of aqueous humor from patients with myopia, Mol. Vis. 14 (2008) 370–377.

[66] J. Shao, Y. Xin, Y. Yao, J. Zhu, Functional analysis of misfolded transthyretin extracted from abnormal vitreous with high myopia related ocular pathologies, Clin. Chim. Acta Int. J. Clin. Chem. 415 (2013) 20–24. doi:10.1016/j.cca.2012.09.006.

[67] T. Bertelmann, W. Sekundo, T. Stief, S. Mennel, Thrombin activity in normal vitreous liquid, Blood Coagul. Fibrinolysis Int. J. Haemost. Thromb. 25 (2014) 94–96. doi:10.1097/MBC.0b013e328364c266.

[68] J. Bastiaans, J.C. van Meurs, V.C. Mulder, N.M.A. Nagtzaam, M. Smits-te Nijenhuis, D.C.M. Dufour-van den Goorbergh, P.M. van Hagen, H. Hooijkaas, W.A. Dik, The role of thrombin in proliferative vitreoretinopathy, Invest. Ophthalmol. Vis. Sci. 55 (2014) 4659–4666. doi:10.1167/iovs.14-14818.

[69] M. Angi, H. Kalirai, S.E. Coupland, B.E. Damato, F. Semeraro, M.R. Romano, Proteomic analyses of the vitreous humour, Mediators Inflamm. 2012 (2012) 148039. doi:10.1155/2012/148039.

[70] C. Hernández, M. García-Ramírez, N. Colomé, L. Corraliza, L. García-Pascual, J. Casado, F. Canals, R. Simó, Identification of new pathogenic candidates for diabetic macular edema using fluorescence-based difference gel electrophoresis analysis, Diabetes Metab. Res. Rev. 29 (2013) 499–506. doi:10.1002/dmrr.2419.

[71] J. Yu, R. Peng, H. Chen, C. Cui, J. Ba, Elucidation of the pathogenic mechanism of rhegmatogenous retinal detachment with proliferative vitreoretinopathy by proteomic analysis, Invest. Ophthalmol. Vis. Sci. 53 (2012) 8146–8153. doi:10.1167/iovs.12-10079.

[72] I. Chowers, R. Wong, T. Dentchev, R.H. Farkas, J. Iacovelli, T.L. Gunatilaka, N.E. Medeiros, J.B. Presley, P.A. Campochiaro, C.A. Curcio, J.L. Dunaief, D.J. Zack, The iron carrier transferrin is upregulated in retinas from patients with age-related macular degeneration, Invest. Ophthalmol. Vis. Sci. 47 (2006) 2135–2140. doi:10.1167/iovs.05-1135.

[73] E. Takahashi, A. Fukushima, A. Haga, Y. Inomata, Y. Ito, M. Fukushima, H. Tanihara, Effects of mechanical stress and vitreous samples in retinal pigment epithelial cells, Biochem. Biophys. Res. Commun. (2016). doi:10.1016/j.bbrc.2016.01.104.

[74] H.P. Gaide Chevronnay, V. Janssens, P. Van Der Smissen, F. N'Kuli, N. Nevo, Y. Guiot, E. Levtchenko, E. Marbaix, C.E. Pierreux, S. Cherqui, C. Antignac, P.J. Courtoy, Time course of pathogenic and adaptation mechanisms in cystinotic mouse kidneys, J. Am. Soc. Nephrol. JASN. 25 (2014) 1256–1269. doi:10.1681/ASN.2013060598.

[75] A. Nykjaer, D. Dragun, D. Walther, H. Vorum, C. Jacobsen, J. Herz, F. Melsen, E.I. Christensen, T.E. Willnow, An endocytic pathway essential for renal uptake and activation of the steroid 25-(OH) vitamin D3, Cell. 96 (1999) 507–515.

[76] H. Appelqvist, P. Wäster, K. Kågedal, K. Öllinger, The lysosome: from waste bag to potential therapeutic target, J. Mol. Cell Biol. 5 (2013) 214–226. doi:10.1093/jmcb/mjt022.

FIGURE LEGENDS

Figure 1: (**A-B**) **Analysis of the vitreous gel.** (**A**) SDS-Page/silver staining of vitreous gel proteins shows similar expression patterns in control and mutant eyes. (**B**) The expression of the major vitreous proteins, collagen II, fibrilin 1, fibronectin is not modified in the mutants (**C**) Experimental work flow for vitreous analysis. The grey coloured boxes depict the standard procedure for biochemical and proteomic analysis of vitreous fluid that may lead to the identification of disease biomarkers, and therapeutic targets (green coloured boxes).

Figure 2: General traits of protein identification. Linear regression obtained by plotting the logarithm of the relative abundance for 2 samples of the same phenotype (Control (C) i vs Cj) (**A**) and for samples from different phenotypes (Mutant (M) I vs Cj) (**B**). (**C**) Venn diagram showing proteins identified in both control and mutant LVF (pale green). The numbers represent the total n umber of proteins identified in each particular dataset.

Figure 3: Interactome of proteins under-expressed in the mutant LVF. The protein-protein interaction network was constructed using String software (version 10, www.string-db.org). The nodes of the network represent the proteins and the lines between them the predicted functional associations. The original graphic was modified to fit the proteins accordingly to their classification in specific biologic pathway: glycolysis and carbohydrate metabolism (colored in orange), citric acid cycle (colored in blue), protein processing in endoplasmic reticulum (colored in purple), actin cytoskeleton regulation (colored in electric blue), neurotrophin pathway (colored in black), proteasome (colored in red), cytochrome P450 system (colored in grey), and phototransduction (colored in green).

Figure 4: Decreased expression of crystallins in mutants. (**A**) Histograms represent the relative quantification for different crystallins identified between control and mutant LVF. Values are mean ± SEM of 3 experiments; *$p<0.05$, **$p<0.01$, ***$p<0.005$. Crystallin beta

A2 (CRBA2); crystallin beta B2 (CRBB2); crystalline beta B3 (CRBB3); crystalline gamma S (CRBS); crystalline gamma C (CRGC). (**B**) Interactome between the different crystallins identified using String software. Crystallin alpha A (CRAA). (C) Interactome of ARF4 including LRP2. ADP-ribosylation factor GTPase-activating protein 1 (ARFGAP1); ADP-ribosylation factor GTPase-activating protein 3 (ARFGAP3); ArfGAP with SH3 domain, ankyrin repeat and PH domain 1 (ASAP1); epidermal growth factor (EGF); EGF receptor (EGFR); Golgi associated, gamma adaptin ear containing, ARF binding protein (GGA3); Lymphoid blast crisis oncogene (LBC); polycystin-1 (PKD1); phospholipase D2 (PLD2).

Figure 5: Interactome of the proteins over-expressed in the mutant LVF. (**A**) The protein-protein interaction was constructed using String software (version 10, www.string-db.org). The original graphic was modified to fit the proteins accordingly to their classification in specific biologic pathway: complement and coagulation pathways (colored in red), transport proteins (colored in green) and immune system (colored in blue). The abbreviations used in the scheme correspond to accessions found in Table S4. Serpina1a (A1AT1); Serpina1b (A1AT2); Serpina1d (A1AT4); Serpin f1 (A2AP); Ahsg (FETUA); A2m (A2M); Pzp (A2MP); Agt (ANGT); Serpinc1 (ANT3); Apoa1 (APOA1); Apoa4 (APOA4); Apoe (APOE); Apoh (APOH); B2m (B2MG); Cpb2 (CBPB2); Cp (CERU); Clu (CLU); C3 (CO3); C4b (CO4B); C9 (CO9); Cfb (CFAB); Cfh (CFAH); Cfi (CFAI); Fn1 (FINC); Gsn (GELS); Hpx (HEMO); Serpind1 (HEP2); Ighg1 (IGH1M); Ighg2c (GCAB); Igh-1a (IGG2B); Ighg3 (IGHG3); Igk-c (IGKC); kng1 (KNG1); Mug1 (MUG1); Serpinf2 (PEDF); Klkb1 (KLKB1); Serping1 (IC1); Plg (PLMN); F2 (THRB); Serpina3m (SPA3M); Trf (TRFE); Alb (ALBU); Ttr (TTHY); and Gc (VTDB); (**B**) Histograms represent the relative quantification for different immunoglobulins identified between control and mutant LVF. Values are mean ± SEM of 3 experiments; *$p<0.05$, **$p<0.01$, ***$p<0.005$.

Figure 6: Interactome of selected proteins over-expressed in the mutant LVF with Lrp2. The protein-protein interaction network was constructed using String software (version 10, www.string-db.org). The nodes of the network represent the proteins, the lines between the marbles represent the predicted functional associations between the proteins. Lrp2 (megalin), A2M (alpha2-macroglobulin), Afm (afamin), Agt (angiotensinogen), Alb (Albumin), Apoa4 (apolipoprotein A-IV), ApoE (apolipoprotein E), Clu (clusterin), Gc (vitamin D binding protein), Sepp1 (selenoprotein P) and Serping1 (plasma protease C1 inhibitor).

Figure 7: Lrp2 deficiency or dysfunction affects epithelial cell morphology. (**A-B**) Transmission electron microscopy micrographs showing the apical junctional complex (AJC) of control and mutant non pigmented epithelium (npe) cells. The AJC between npe cells (arrowheads) contains a tight junction (tj) followed by a large adherent junction (aj) in both normal (**A**) and Lrp2cKO (**B**) ciliary epithelium. (**C-D**) Confocal images showing the expression of occludin in endothelial cells of the ciliary microvasculature (cm) and at the pe-npe interface in both normal (**C**) and Lrp2cKO (**D**) ciliary epithelium. (**E**) Transmission electron micrographs showing rod outer segments (os) interacting with the long microvilli of the retinal pigmented epithelium (RPE) in a normal photoreceptor layer (prl). (**F**) In control eyes, the AJC between RPE cells contains a long TJ followed by a large AJ (arrowheads). (**G**) In Lrp2cKO eyes, the prl is greatly modified, outer segments are absent and the microvilli are hypotrophic (arrow). (**H**) Higher magnifications showing the disorganized and hypotrophic microvilli in Lrp2cKO RPE cells. (**I-J**) In Lrp2cKO RPE cells, the AJC (arrowheads) is modified, the rarely found TJs are smaller (**I**), poorly defined or absent (**J**). (**K-L**) Ectopic expression of the alpha-smooth muscle actin in the RPE of Lrp2cKO retina (white arrows). (**M**) alpha smooth-muscle actin, alpha chain collagen 1, ZO-1, and phospho-Erk1/2. The level of endogenous total ERK is shown for comparison. GAPDH is used as loading control. (**N**) Immunoblot analysis of control and mutant RPE extracts for early endosome antigen 1

(EEA1), cathepsin-D (Cath-D), and lysosome membrane protein 2 (LIMP2). GAPDH is used as loading control. (**O**-**P**) *In vivo* injection of fluorescent albumin. (**O**) In the normal eye, albumin is located in endothelial cells of the choroid and inner retinal vasculature, and in clearly defined vesicles at the level of the RPE layer (arrows). (**P**) In the mutant eye, albumin is no more visible in endothelial cells of the sclera and RPE cell layer. Endocytic vesicles are almost completely absent. (**Q**) Immunoblot analysis of control and mutant, retina and, RPE extracts for ADP ribosylation factor 4 (Arf4) and ras-related protein rab11 (rab11). (**R**) Co-immunoprecipitation of Lrp2 and Arf4. bm: Brusch membrane; pe: pigment epithelium; rpe: retinal pigment epithelium. Scale bars: 500 nm in A, B; 30 μm in C, D; 3 μm in E, G; 800 nm in F, H, I, J; 90 μm in K, L; 50 μm in O, P.

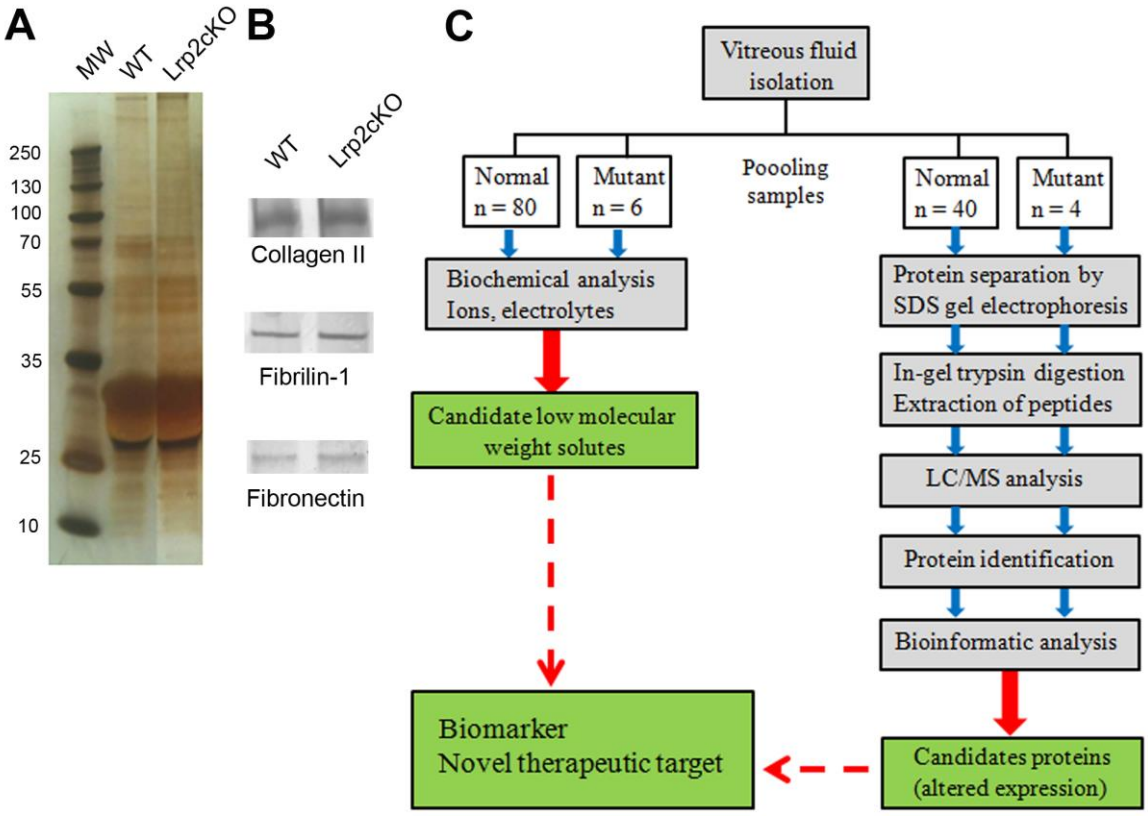

Figure 1

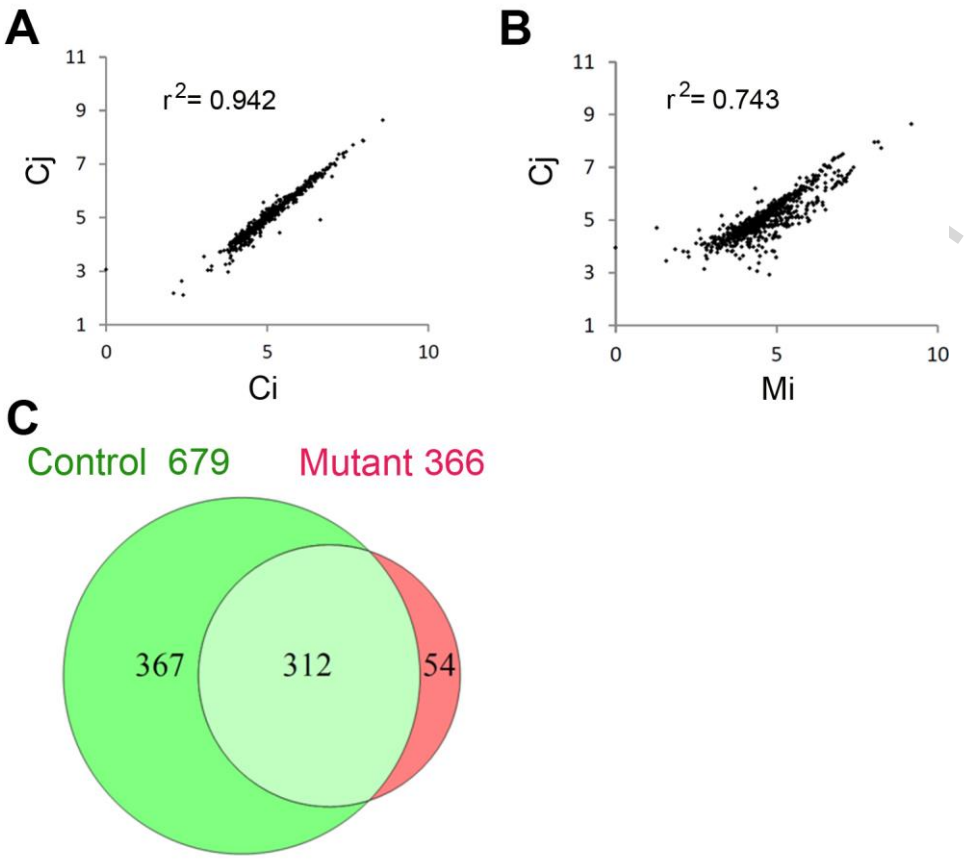

Figure 2

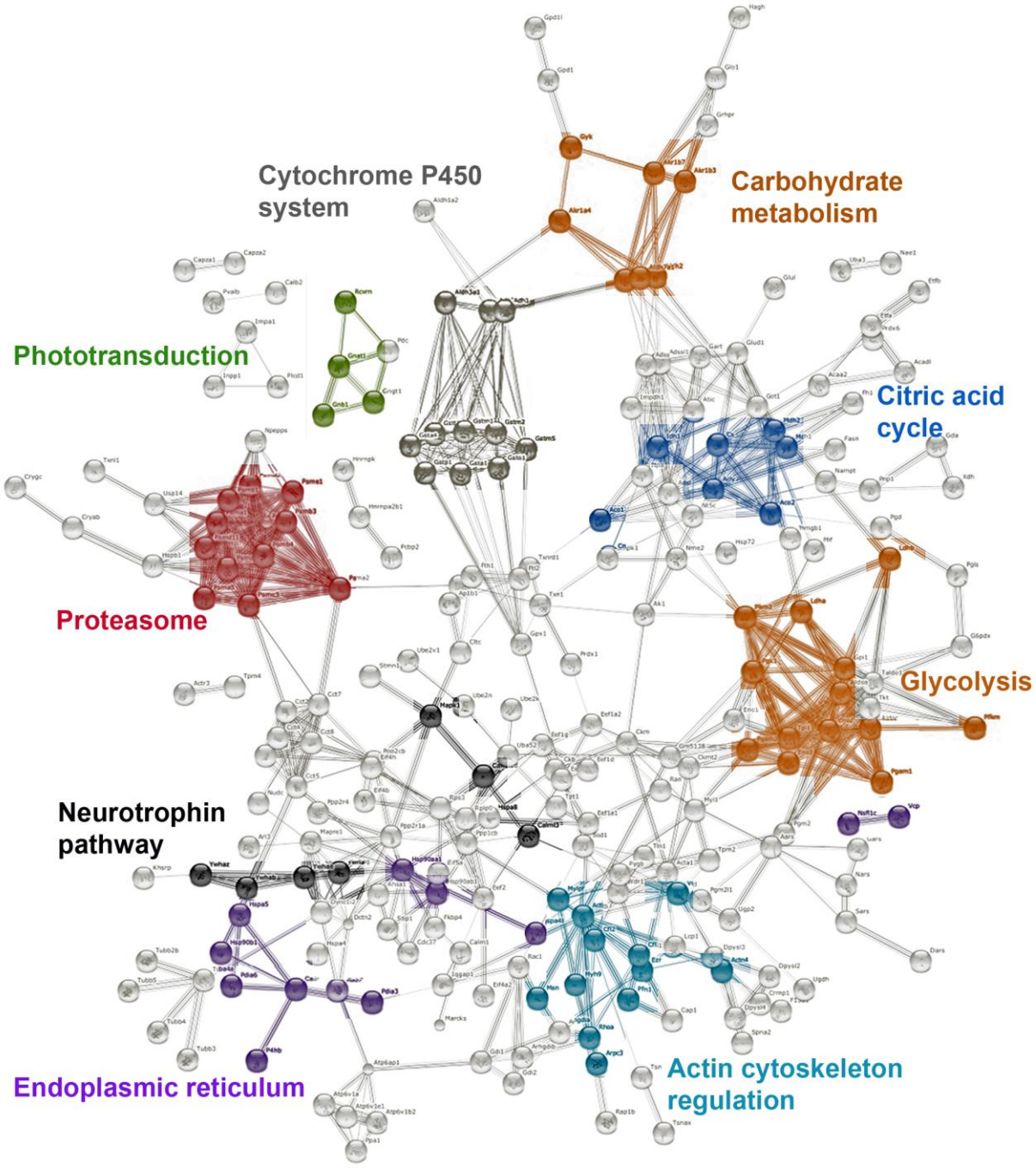

Figure 3

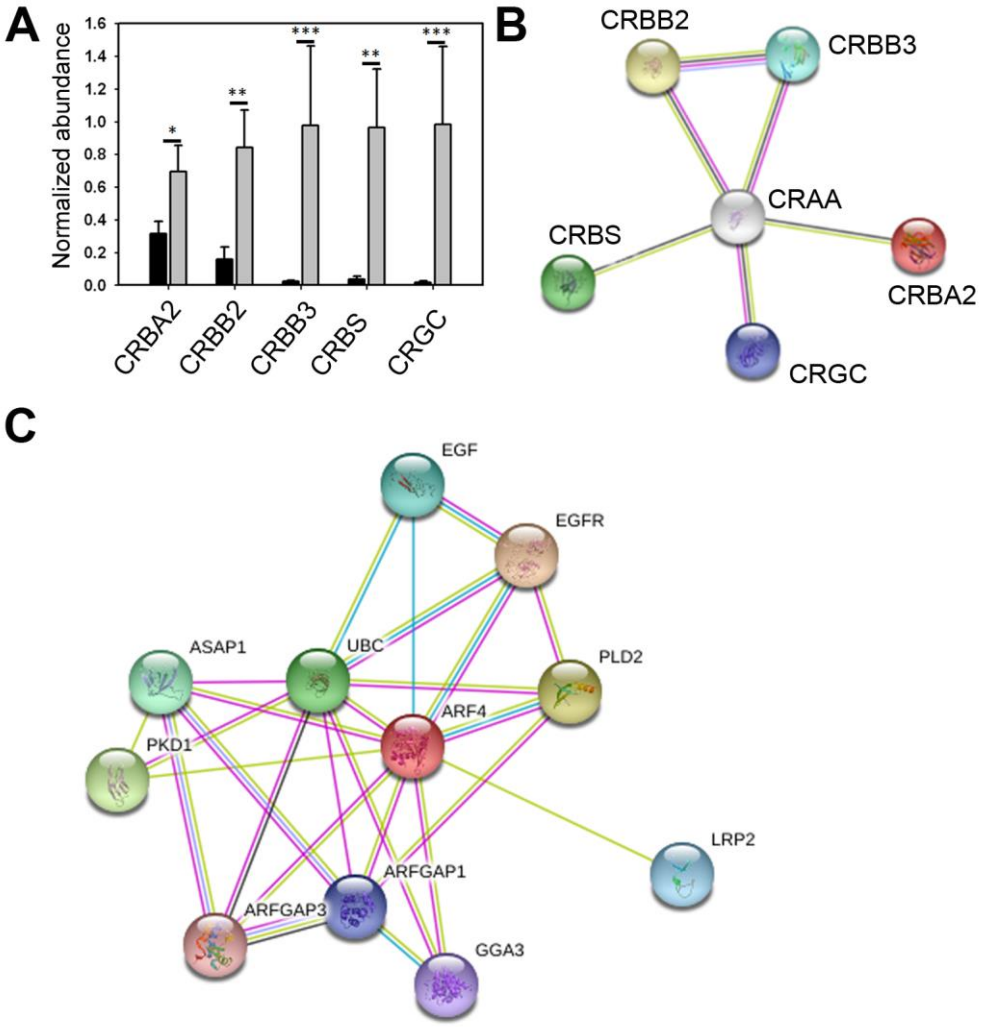

Figure 4

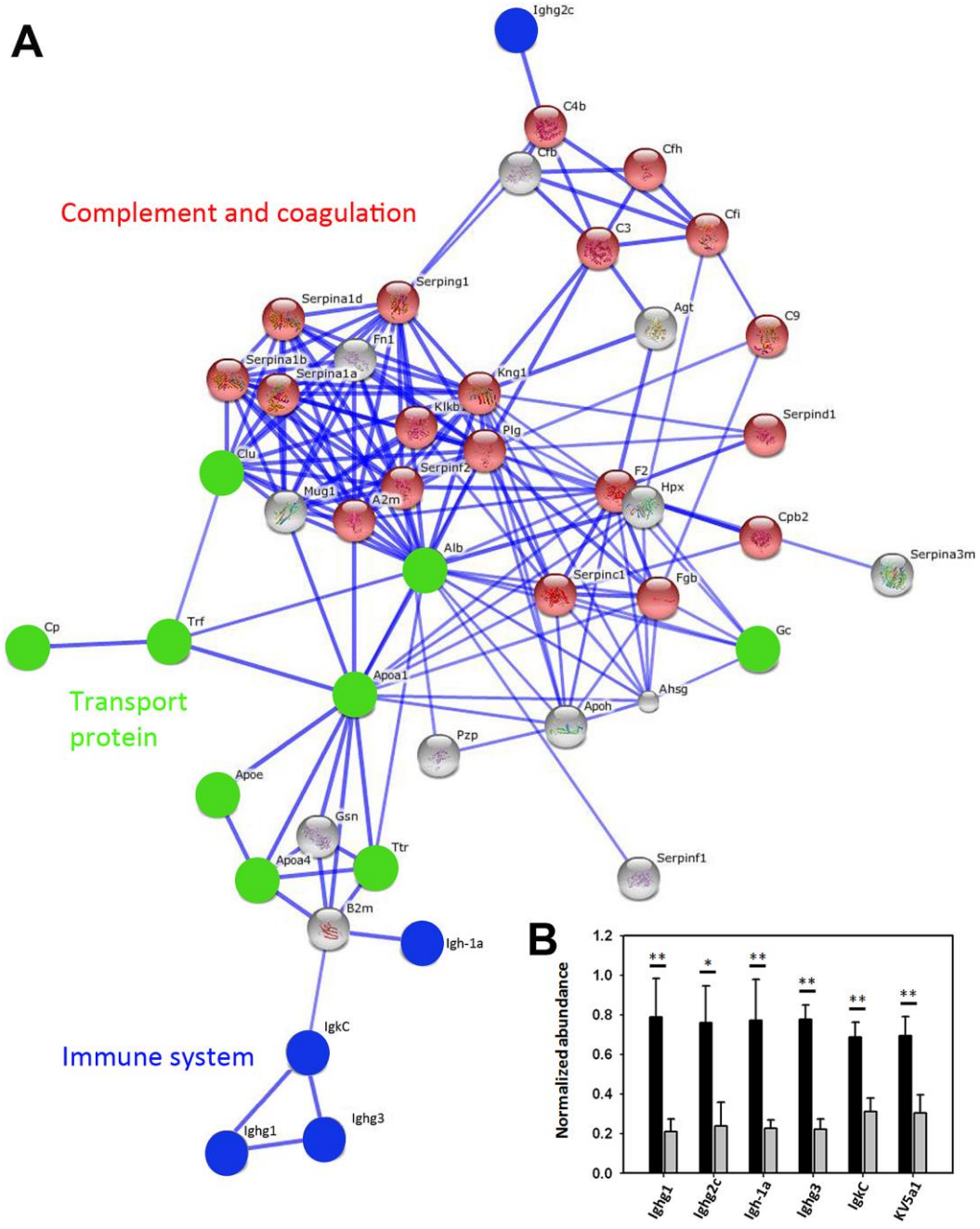

Figure 5

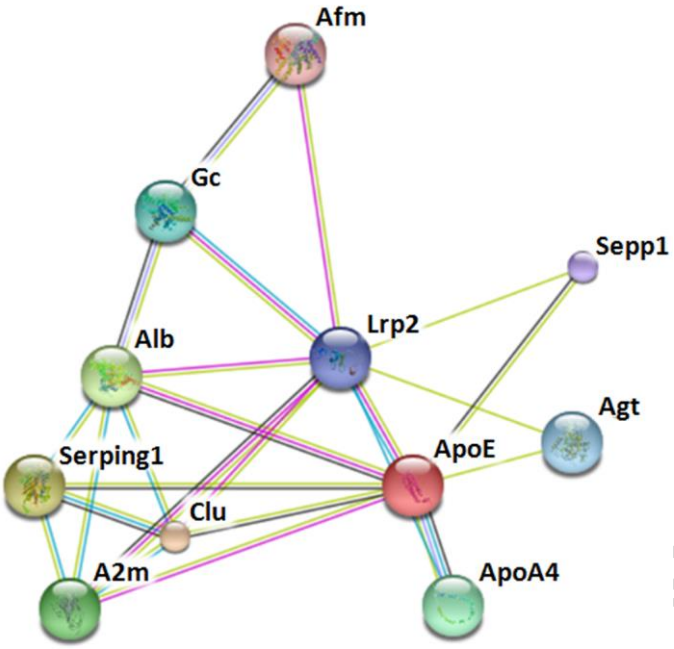

Figure 6

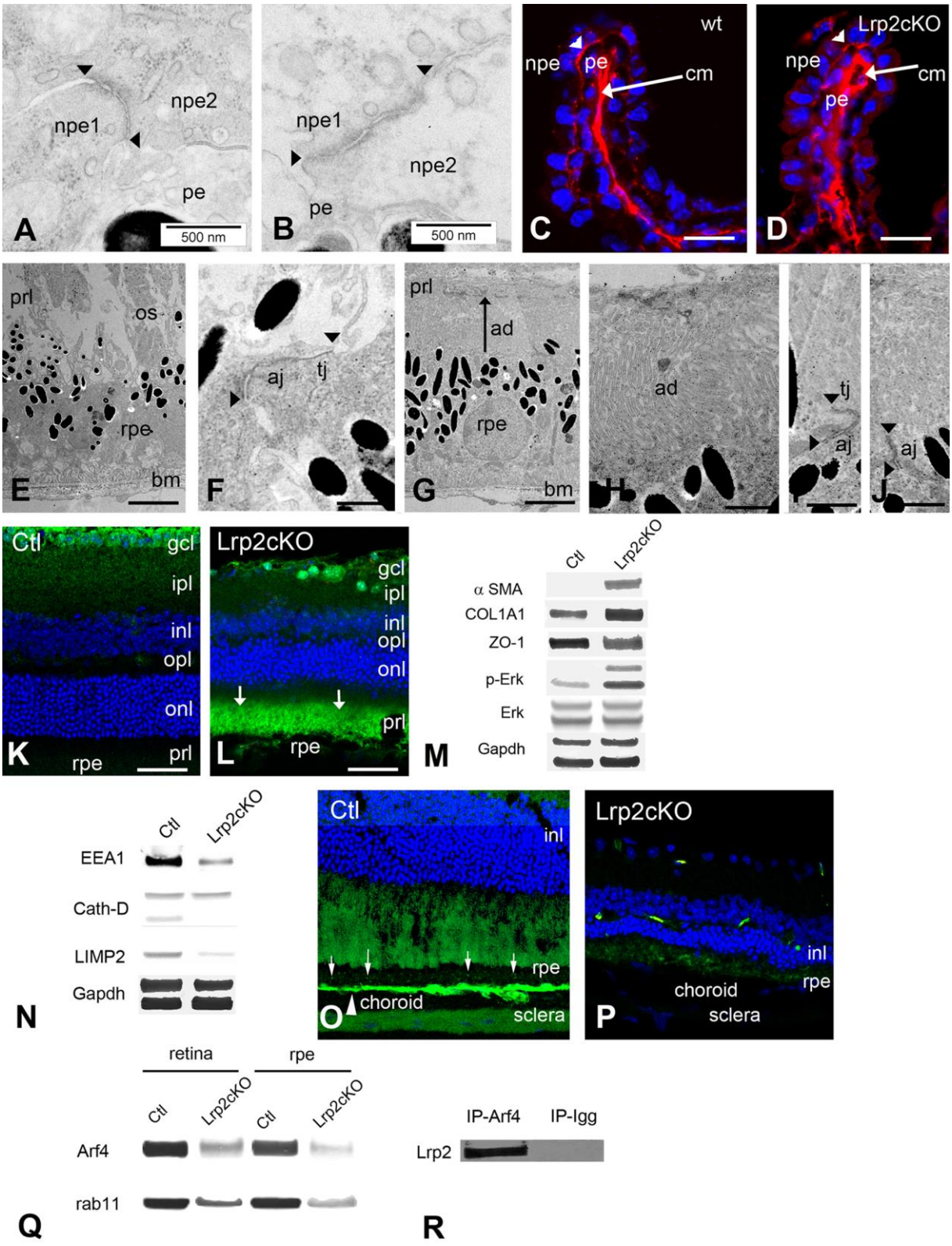

Figure 7

Highlights

- Proteomic and ionic analysis of vitreous uncover novel biomarkers in high myopia
- Pathogenic retinal pigment epithelium is a main actor in high myopia
- Eye growth relies on a protein network in which LRP2 is an essential component